25-hydroxycholesterol inhibits human papillomavirus infection in cervical epithelial cells by perturbing cytoskeletal remodeling

Boning Li[1], Chen Hua[2], Pu Tian[1], Yiou Sha[2], Lu Zhang[1], Qian Wang[2], Lu Lu[2], Shibo Jiang[2], and Long Sui[1]

[1]Obstetrics and Gynecology Hospital of Fudan University
[2]Fudan University School of Basic Medical Sciences

January 27, 2023

Abstract

Persistent high-risk human papilloma virus (HR-HPV) infection is the main risk factor for cervical cancer, threatening women's health. Despite growing prophylactic vaccination, annual cervical cancer cases are still increasing and show a trend of younger onset age. However, therapeutic approaches towards HPV infection are still limited. 25-hydrocholesterol (25HC) has a wide-spectrum inhibitory effect on a variety of viruses. To explore efficient interventions to restrict HPV infection at an early time, we applied different pseudoviruses (PsV) to evaluate anti-HPV efficacy of 25HC. We tested PsV inhibition by 25HC in cervical epithelial-derived HeLa and C-33A cells, using high-risk (HPV16, HPV18, HPV59), possibly carcinogenic (HPV73), and low-risk (HPV6) HPV PsVs. Then we established murine genital HPV PsV infection models and applied IVIS to evaluate anti-HPV efficacy of 25HC *in vivo*. Next, with the help of confocal imaging, we targeted 25HC activity at filopodia upon HPV exposure. After that, we used RNA-seq and Western blotting to investigate 1) how 25HC disturbs actin cytoskeleton remodeling during HPV infection and 2) how prenylation regulates the cytoskeletal remodeling signaling pathway. Our findings suggest that 25HC perturbs F-actin rearrangement by reducing small GTPase prenylation. In this way, the phenomenon of HPV virion surfing was restricted, leading to failed infection.

25-hydroxycholesterol inhibits human papillomavirus infection in cervical epithelial cells by perturbing cytoskeletal remodeling

Running Title: 25-HC inhibits HPV by perturbing cytoskeleton

Boning Li[1, 2, *], Chen Hua[3, *], Pu Tian[1, 2, *], Yiou Sha[3], Lu Zhang[1, 2], Qian Wang[3], Lu Lu[3, #], Shibo Jiang[3, #], Long Sui[1, 2, #]

[1]The Obstetrics and Gynecology Hospital of Fudan University, Shanghai, 200011, China

[2]Medical Center of Diagnosis and Treatment for Cervical Diseases, Obstetrics and Gynecology Hospital of Fudan University, Shanghai, 200011, China

[3] Key Laboratory of Medical Molecular Virology (MOE/NHC/CAMS), School of Basic Medical Sciences, Shanghai Institute of Infectious Disease and Biosecurity, Fudan University, Shanghai, China

* These authors contributed equally to the study.

#Corresponding authors: Lu Lu (lul@fudan.edu.cn), Shibo Jiang (shibojiang@fudan.edu.cn), Long Sui (suilong@fudan.edu.cn)

Abstract

Persistent high-risk human papilloma virus (HR-HPV) infection is the main risk factor for cervical cancer, threatening women's health. Despite growing prophylactic vaccination, annual cervical cancer cases are still increasing and show a trend of younger onset age. However, therapeutic approaches towards HPV infection are still limited. 25-hydrocholesterol (25HC) has a wide-spectrum inhibitory effect on a variety of viruses. To explore efficient interventions to restrict HPV infection at an early time, we applied different pseudoviruses (PsV) to evaluate anti-HPV efficacy of 25HC. We tested PsV inhibition by 25HC in cervical epithelial-derived HeLa and C-33A cells, using high-risk (HPV16, HPV18, HPV59), possibly carcinogenic (HPV73), and low-risk (HPV6) HPV PsVs. Then we established murine genital HPV PsV infection models and applied IVIS to evaluate anti-HPV efficacy of 25HC *in vivo* . Next, with the help of confocal imaging, we targeted 25HC activity at filopodia upon HPV exposure. After that, we used RNA-seq and Western blotting to investigate 1) how 25HC disturbs actin cytoskeleton remodeling during HPV infection and 2) how prenylation regulates the cytoskeletal remodeling signaling pathway. Our findings suggest that 25HC perturbs F-actin rearrangement by reducing small GTPase prenylation. In this way, the phenomenon of HPV virion surfing was restricted, leading to failed infection.

Keywords: human papilloma virus, 25-hydrocholesterol, cytoskeleton, filopodia, prenylation

Introduction

Cervical cancer ranks fourth as the most common malignant tumors in women. Persistent high-risk human papilloma virus (HR-HPV) infection is the major risk factor of cervical epithelial cancer. Most women undergo at least one HPV infection in their lifetime, and an estimated 10% will go on to develop squamous intraepithelial lesions (SILs), followed, in some cases, by cervical cancers arising from high-grade squamous intraepithelial lesions (HSILs)(1). Prophylactic vaccines have made remarkable achievements in preventing HR-HPV infection and the occurrence of cervical cancer (2). However, vaccines cannot account for all HR-HPV types, and more than 500,000 new cervical cancer cases are still diagnosed annually, causing 300,000 deaths every year (3). Currently, the mechanisms underlying the invasion of HPV into host cells and its ability to escape immune surveillance remain to be elucidated. For this reason, progress in developing medications and therapeutic vaccines is lagging, and efficient interventions for persistent HPV infection are lacking. This calls for intensified investigation to gain more insight into HPV behavior pursuant to developing a broad-spectrum strategy for early control of HPV infection.

25-hydroxycholesterol (25HC) is an effector of IFN signaling; it is catalyzed from cholesterol by a product of interferon stimulated gene (ISG), termed cholesterol 25-hydroxylase (CH25H)(4). 25HC exerts inhibitory power against a wide-spectrum of viruses, including vesicular stomatitis virus (VSV), herpes simplex virus (HSV), human immunodeficiency virus (HIV), murine P51 gammaherpesvirus 68 (MHV68), Ebola virus (EBOV), Rift Valley fever virus (RVFV) and Russian spring-summer encephalitis virus (RSSEV)(5). In addition, it is recently reported that 25HC potently suppressed SARS-Cov-2 replication (6). Nevertheless, whether 25HC could act as an antiviral restriction factor for multiple HPV types remains unclear.

Considering this last point, we herein aimed to demonstrate whether 25HC could inhibit HPV infection in cervical epithelial cells in a broad-spectrum way, probing the etiological mechanisms in a parallel manner. As a result, we can report a lipid metabolism-related mechanism of 25HC antiviral efficacy against HPV. More specifically, 25HC inhibited HPV entry by restricting prenylation of small GTPases in cervical epithelial cells, thereby impeding formation of filopodia, which is essential for HPV virion surfing.

Materials and methods

Cell lines and reagents

Human cervical carcinoma cells (HeLa and C-33A) and human embryonic kidney cell line (293FT) were purchased from the Chinese Academy of Sciences Cell Bank (Shanghai, China). Cells were cultured in high-glucose Dulbecco's modified Eagle's medium (DMEM) (HyClone, Utah, USA) supplemented with 10% fetal bovine serum (FBS) (Yeasen, Shanghai, China), and incubated in a humidified environment containing 5% CO2 at 37°C. 25HC (MedChemExpress, Shanghai, China) was first dissolved in ethanol and diluted to

working concentrations with DMEM. The final concentration of solvent in the medium was <0.1%. 25HC, FTI277 and GGTI298 were purchased from MedChemExpress (Shanghai, China).

PsV production

HPV PsVs were produced as described previously (7). Briefly, 293FT cells were seeded in a T-75 flask the day before transfection to reach 70%-80% cell density. Then, the cells were transfected with a mixture of HPV-L1/L2-expressing plasmid (p6sheLL, p16sheLL, p18sheLL, p59sheLL or p73sheLL) and pCLucf plasmid using Lipofectamine 2000 reagent (Solarbio, Beijing, China). The cells were suspended in 0.5 mL of lysis buffer and incubated overnight at 37°C. The lysate was cooled on ice for 15 min and then centrifuged at 5,000 rpm for 5 min at 4°C. The pseudovirion stock was stored at -80°C.

HPV inhibition assay

HeLa or C-33A cells were seeded at 10^4 cells/well on a 96-well plate 12 h prior to infection. 25HC or other reagents were serially diluted in DMEM and incubated with HPV PsV. Mixtures were added to cells and incubated at 37°C for 16 h. After washing with PBS, cells were maintained in DMEM with 1% FBS for an additional 72h. Then, cells were lysed, and infectivity was measured by quantitative luciferase assay, according to the manufacturer's manual (Promega Madison, WI, USA).

Time-of-addition assay

HeLa cells were seeded in wells of a 96-well cell culture plate overnight. Then cells were treated with 25HC in the final concentration of 10 μM at 20 h and 4 h before or 0 h, 2 h, 6 h, and 8 h after HPV6, HPV16, HPV18, HPV59 or HPV73 PsV addition. The medium was changed to 1 % FBS 16 h post-PsV inoculation. Luciferase activity was measured after 72 h to assess inhibitory ratio**(Figure 3Aa)** .

Pretreatment assay

HeLa cells in a 96-well plate were preincubated with serially diluted 25HC for 12 h, or preincubated with 10 μM 25HC for different time periods. Then cells were washed with PBS thoroughly and inoculated with HPV6, HPV16, HPV18, HPV59 or HPV73 PsV. After 16 h, the medium was changed to 1% FBS, and luciferase assay was performed 72 h after inoculation**(Figure 3Ab)** .

Inactivation assay

25HC-mediated HPV inactivation activity was determined as previously described (7, 8). Briefly, HPV16 PsV was incubated with 25HC at room temperature for 1 h and then subjected to repurification by centrifugation through a 100k ultrafiltration spin-column 3 times; otherwise, PEG-8000 (3%) was added to precipitate the virus at 4°C for 1 h. Next, the protein-virus mixture was centrifuged at 12,000 rpm for 30 min and washed 3 times. The separated PsVs were used to infect HeLa cells, and luciferase was detected 72 h post-infection, as described previously.

Immunofluorescence staining and confocal imaging

To evaluate intracellular HPV16 PsV, HeLa cells were plated on coverslips, inoculated with HPV16 PsV and treated with 25HC or vehicle as indicated in the figure legends. Cells were fixed in 4% paraformaldehyde (PFA), permeabilized by 0.1% Triton-X, and blocked with 3% BSA. After that, cells were incubated with anti-HPV16 L1 antibody (Abcam, UK) at 4 degC overnight. The next day, cells were incubated with FITC-labeled goat anti-mouse IgG (Yeasen, Shanghai, China) and sealed with mounting medium containing DAPI (Yeasen, Shanghai, China). Fluorescent images were captured with a fluorescence microscope (Olympus).

To analyze microfilament morphology, cells were pretreated with 25HC or vehicle 12 h before shifting to 4 degC and inoculating with HPV16 PsV. Cells were kept for 2 h at 4 degC and then immediately washed with cold PBS and shifted back to 37 degC. At 0 min, 5 min, 30 min, 1h and 2 h after shifting to 37 degC, cells were fixed with PFA. Rhodamine-Phalloidin was used to stain F-actin. After sealing with mounting medium, coverslips were scanned with a confocal microscope equipped with a 63 x objective lenses (Leica, TCS SP8).

Mouse model and HPV PsV challenge

Sexually mature 6- to 8-week-old female Balb/c mice were obtained from the Silaike Corporation (Shanghai, China). Mice were allowed to adapt to the new environment for at least a week and were maintained in SPF conditions. All animal procedures were approved by the Institutional Animal Care and Use Committee of Shanghai and were performed in accordance with the National Research Council Guide for the Care and Use of Laboratory Animals.

The establishment of a genital HPV PsV infection model was performed in accordance with previous literature (9). Briefly, all mice received 3mg of Depo-Provera (Pfizer) in a subcutaneous injection at day 0. For vaginal challenge, the mice were intravaginally instilled with nonoxynol-9 at day 4. Six h later, HPV16 PsV was inoculated after mechanical disruption of the genital tract by a cytobrush. Mice were pretreated intravaginally with 25HC (0.1 μmol) before PsV infection. After 2 days, *in vivo* luciferase expression was measured, according to the manufacturer's protocols (Promega Madison, WI, USA), and imaging was performed using an IVIS spectrum imaging system.

Western blot analysis and antibodies

HeLa cells were seeded in wells of a 6-well cell culture plate. To analyze the LIMK/cofilin signaling pathway, HeLa cells were treated in a manner consistent with that in confocal imaging. At the corresponding time points, cells were lysed in RIPA lysis buffer with 1 × protease inhibitor and 1 × phosphatase inhibitor. Membrane proteins were separated using a Membrane and Cytosol Protein Extraction Kit (Yeasen, Shanghai, China). Proteins in lysates were resolved by SDS-PAGE and transferred to PVDF membranes. Proteins were probed with indicated primary antibodies. Anti-LIM Kinase1 antibody, Anti-LIM Kinase 1 (phospho T508) antibody, anti-Cofilin (phospho S3) antibody and anti-cofilin antibody were purchased from Abcam (UK). β-actin (Proteintech, USA) and GAPDH (Proteintech, USA) were used as loading controls for total protein; ATP1A1 (Proteintech, USA) was used as a loading control for membrane proteins. Blots were visualized using an Enhanced ECL Chemiluminescent Substrate Kit (Yeasen, Shanghai, China), and band intensity was quantified with ImageJ software.

Small GTPase activity assay

Activation of RhoA, Rac1 and Cdc42 was measured using a RhoA/Rac/Cdc42 Activation Assay Combo Biochem Kit (Cytoskeleton, USA), according to the manufacturer's manual. In brief, Rhotekin-RBD or PAK-PBD affinity beads were added to the cell lysates, and GTPase activity was analyzed by pull-down assay with specific antibodies on a Western blot.

Rap1 activity was tested by measuring active Rap1-GTP level with a Rap1 Activation Assay Kit (NewEast Biosciences, USA). Rap1-GTP in cell lysates was incubated with anti-active Rap1 antibody, and then the bound active Rap1 was pulled down by protein A/G agarose, followed by immunoblot detection.

RNA sequencing (RNA-seq) and bioinformatics analysis

10 μM 25HC or vehicle was added to HeLa cells for 12 h. Three biological replicates of control and 25HC-treated group were used for RNA-seq. Total RNA was isolated using the EZ-press RNA Purification Kit (EZBioscience), according to the manufacturer's instructions. The quality of RNA was analyzed using the NanoDrop spectrophotometer and Agilent 2100 bioanalyzer (Thermo Fisher, Waltham, MA, USA). RNA-seq was performed on a DEBSEQ platform (BGI-Shenzhen, China).

Differential expression analysis was performed using the DESeq2 (v1.4.5) with Q value [?] 0.05 and |log2FC| [?] 1.5. The heatmap was drawn by pheatmap (v1.0.8), according to the gene expression in different samples. GO and KEGG enrichment of annotated differentially expressed genes (DEGs) was performed by Phyper based on ahypergeometric test. Significance levels of terms and pathways were identified with a Q value [?] 0.05. Gene set enrichment analysis (GSEA) of total gene list was performed by GSEA software. Enriched gene sets were assigned based on |NES| [?] 1, p-value[?] 0.05, FDR q-value [?]0.25.

Quantitative real-time PCR (qPCR)

Total RNA was extracted from control and 25HC-treated samples, as shown in RNA sequencing. qPCR was performed by using TB Green Premix Ex Taq II (Takara) in a CFX96 Real-Time PCR Detection System (BioRad, Munich, Germany). Relative mRNA expression levels were calculated according to ΔΔCt upon normalization to *GAPDH* expression. The primer sequences used for mRNA detection were as follows: 5'- TGTGACCGGCAAAATTGGC -3' (F) and 5'- GCCCGTTGCAGACACTGAA -3' (R) for *FDPS* ; 5'- ACAGCATCTATGGAATCCCATCT -3' (F) and 5'- CAAAAGCTGGCGGGTAAAAAG -3' (R) for *GGPPS* .

Results

25HC is a potent inhibitor against HPV entry into cervical epithelial cells

We produced HPV6, HPV16, HPV18, HPV59 and HPV 73 PsVs to evaluate the inhibitory activity of 25HC against infection of multiple HPV types. Of these HPV types, HPV6 is a low-risk type, which causes benign genital warts; HPV16, HPV18 and HPV59 are recognized as high-risk types, causing cervical cancer, and HPV73 is defined as a possible carcinogenic type (10). PsV inhibition experiments were performed in HeLa cells and C-33A cells, both of which are human cervical epithelial-derived cancer cell lines. 25HC was serially diluted and incubated with HPV PsV. The mixture was then added to HeLa or C-33A cells. As shown in **Figure 1A** , 25HC exhibited marked anti-HPV activity in a dose-dependent fashion in both HeLa and C-33A cells. Moreover, the anti-HPV activity of 25HC was not type-restricted, with IC50 (half maximal inhibitory concentration) values falling in the low micromolar range. For almost all HPV subtypes, IC90 of 25HC was less than 20 μM. These results suggest that 25HC is effective against various HPV subtypes in cervical epithelial cells.

For better visualization of HPV entry-inhibition of 25HC, we performed immunofluorescence staining to examine the internalization of HPV16 PsV post-infection (**Figure 1B**). HPV16 PsV virions were marked by antibody against L1 protein; however, with 25HC incubation, few PsV virions were detected intracellularly. Taken together, 25HC effectively inhibited HPV infection in human cervical epithelial cells.

25HC inhibited genital HPV16 infection *in vivo*

To explore the *in vivo* efficacy of 25HC, we established murine genital infection models using HPV16 PsVs. Genital infection with PsV expressing luciferase was detected by measuring bioluminescence with the IVIS system, and the luminescent signal intensity was calculated (9). 25HC was perfused in the murine vaginal tract before PsV challenge. Vaginal administration of 25HC conferred complete protection against murine genital HPV PsV infection and significantly reduced luciferase titration (**Figure 2AB**). In conclusion, 25HC possessed inhibitory effects on HPV infection *in vivo* , and intravaginal treatment might be an efficient route of medication.

25HC targeted cervical epithelial cells at an early stage of HPV infection

In order to determine the specific mechanism of 25HC inhibitory effect, we performed a time-of-addition assay **(Figure 3Aa)** . 25HC exerted a high anti-HPV efficacy (> 80%) when added to cells 20 h before infection, 4 h before infection, or at the moment of infection. However, when 25HC treatment was applied 2 h after viral infection or later, we observed a sharp drop in its antiviral efficacy**(Figure 3C)** . This result suggests that 25HC might affect the early steps of HPV infection.

We next investigated whether 25HC targeted virus or cervical epithelial cells. To make this determination, HeLa cells were pretreated with serial dilutions of 25HC for 12 h, and then the compounds were removed and PsVs were added to cells **(Figure 3Ab)** . HPV6, HPV16, HPV18, HPV59 and HPV 73 were all inhibited by 25HC pretreatment in a dose-dependent manner**(Figure 3D)** . In addition, we pretreated HeLa cells with 10 μM 25HC for different time periods. HPV PsVs were also inhibited in a time-dependent manner **(Figure 3E)** . The pretreatment assays imply that 25HC modifies cell biological processes to render cells less susceptible to HPV.

To determine whether 25HC could inactivate HPV PsV, we incubated HPV16 PsV with 25HC for 1 h at

room temperature and then separated by ultrafiltration. The PsVs were resuspended and added to HeLa cells to analyze infection activities. However, 25HC had little effect on HPV PsV activity **(Figure 3B)** . Taken together, we speculate that 25HC targets cervical epithelial cells, but not HPV, to inhibit infection.

25HC suppressed filopodia formation during HPV virion surfing

As shown in **Figure 4A,** HPV transports along filopodia in a manner previously termed as "virion surfing" (11). Through this form of physical movement, virions locate on cellular receptors and are uptaken into cytoplasm by long, finger-like, actin-rich protrusions (12). The filopodium is a cytoskeletal structure formed by actin filaments. To describe the arrangement of fibrous actin (F-actin) of HeLa cells during HPV16 PsV infection, we stained the cells with rhodamine-phalloidin to visualize the actin network. In accordance with previous studies, the cortical actin cytoskeleton could be rapidly reorganized by its highly dynamic behavior upon the exposure of cervical epithelial cells to HPV particles (13). The remodeling of F-actin could be visualized fewer than 5 min post-infection. We observed long and abundant filopodia at the cell edge via confocal photomicroscopy. The strong induction of filopodia extended beyond 30 min post-infection, and a thorough dissolution took place within 2 h **(Figure 4B)** . However, with pretreatment of 25HC, no obvious filopodium structure was activated by HPV16 PsV, and F-actin appeared diffuse **(Figure 4C)** . We infer from these results that 25HC suppresses HPV virion surfing by disrupting F-actin remodeling.

25HC perturbed F-actin remodeling by interfering with small GTPase/LIMK/cofilin signaling

To elucidate the mechanism underlying 25HC regulation of actin dynamics, we investigated the signaling pathway involved in filopodia formation. The actin-depolymerizing factor (ADF)/cofilin family proteins play pivotal roles in actin filament dynamics and reorganization. LIM kinase (LIMK) modulates cofilin activity by phosphorylating serine residue 3 (Ser-3), and it is activated by phosphorylation of conserved threonine residue. To evaluate the activation of LIMK-cofilin signaling, we detected the level of LIMK1 and cofilin phosphorylation by Western blotting. As demonstrated in **Figure 5A** , total cofilin and LIMK1 protein levels did not display obvious alterations. Cofilin was phosphorylated drastically post-infection, and the phosphorylation level gradually decreased from 30 min post-infection up to 2 h post-infection (**Figure 5AB)** . The trend of cofilin phosphorylation was similar to the kinetics of filopodia. In addition, p-LIMK1 remained increased by the stimuli of HPV16 PsV infection. However, for the 25HC-treated group, the phosphorylation of cofilin and LIMK1 was suppressed at every time point (**Figure 5AC)** . These results indicate an intense inhibition towards LIMK/cofilin phosphorylation by 25HC.

Small molecular weight GTPases (small G proteins, or small GTPases) are essential for cell signal transduction. Among them, the Rho family plays a major role in controlling cytoskeletal dynamics, widely reported as upstream of LIMK/cofilin. Rap1 GTPase, which is a member of the Ras subfamily, is also reported to be involved in actin organization (14, 15). To validate whether 25HC hampers actin remodeling by inactivating small GTPases, we measured GTP-bound Rho GTPases by a pull-down assay, as well as GTP-bound Rap1 by co-IP assay. According to **Figure 5D** , 12-h treatment of 25HC reduced GTP-Rac1, GTP-Cdc42, GTP-RhoA and GTP-Rap1. Such evidence strongly suggests that 25HC suppresses small GTPase activity to inhibit LIMK/cofilin phosphorylation.

25HC regulated lipid metabolism in HeLa cells

To further explore how 25HC inhibited Rap and Rho activity, we performed RNA sequencing from HeLa cells treated with 25HC. With a threshold of $|\log2FC| >= 1.5$ and Qvalue $<= 0.05$, we identified 67 differentially expressed genes (DEGs)**(Figure 6A)** . To characterize the functions of DEGs, we conducted functional annotation analysis, using Gene Ontology (GO) analysis (biological process) and Kyoto Encyclopedia of Genes and Genomes (KEGG) Pathway mapping. The enriched gene sets presented lipid metabolism-related terms. Specifically, 20 gene sets, including "cholesterol biosynthetic process", "sterol biosynthetic process" and "isoprenoid biosynthetic process", were enriched by GO analysis. Then, "steroid biosynthesis" and "terpenoid backbone biosynthesis" were enriched according to KEGG mapping **(Figure 6 BC)** . Next, to prevent a biased conclusion based on only DEGs, we evaluated general differences in the cumulative distribution of total gene expression via Gene Set Enrichment Analysis (GSEA) based on GO (biological

process). We found that the 25HC-treated group negatively enriched 23 gene sets. Most of these gene sets were also related to lipid metabolism **(Table 1)** . 25HC seems to be a negative lipid metabolism regulator, which is consistent with previous studies (16).

25HC inhibited the synthesis of protein prenylation substrates

We noticed that downregulation of "isoprenoid biosynthetic process" was represented in both GO analysis and GSEA analysis **(Figure 6D)** . According to data from RNA-seq, most genes in this term were significantly downregulated by 25HC **(Figure 6E)** . Isoprenoids are required for protein prenylation, which is a typical post-translational modification of small GTPases. The two forms of prenylation are farnesylation and geranylgeranylation, ensuring that small GTPases' function appropriately as signaling switches. In mammalian cells, isoprenoids are only produced by the mevalonate (MVA) pathway (17). We analyzed RNA-seq data for gene expression of the enzymes involved in MVA, and most of them decreased in 25HC-treated cells **(Figure 7F)** . In addition, we verified the gene expression of key enzymes for prenylation substrates (farnesyl diphosphate (FPP) and geranylgeranyl diphosphate (GGPP)) by qPCR. Again, 25HC significantly reduced mRNA expression of farnesyl diphosphate synthase (*FDPS*) and geranylgeranyl diphosphate synthase (*GGPPS*) (18). *FDPS* level was only one-third that of the control group **(Figure 6G)** . In conclusion, both RNA-seq and qPCR results illustrate that 25HC impeded the synthesis of prenylation substrates.

25HC restricted small GTPase prenylation in cervical epithelial cells

We used a pan-farnesylation antibody to assess the general prenylation state in HeLa cells. As expected, pan-farnesylation level was downregulated in 25HC-treated cells **(Figure 7A)** . Next, because prenylation determines subcellular sorting of proteins, we separated membrane proteins to evaluate Rac1, Cdc42, RhoA and Rap1 protein localized to membrane compartments. Membrane-bound small GTPases were reduced by 25HC, indicating less prenylation status. These observations support the decrease in isoprenoids synthesis by 25HC as a factor contributing to the restriction of small GTPase prenylation**(Figure 7B)** .

Inhibition of prenylation by 25HC hampered HPV infection

To confirm whether restraint of prenylation hampers HPV infection, we inoculated HeLa cells with HPV16 PsV and treated them with inhibitors of farnesyl transferase (FTase) or geranylgeranyl transferase (GGTase) at the same time. Exposure of prenylation inhibitors revealed a dose-dependent inhibition of HPV16 PsV **(Figure 7C)** . We also co-treated HPV16-infected HeLa cells with 25HC and the farnesylation substrate FPP. Exogenous addition of FPP restored infectivity of HPV16 PsV in the presence of 25HC **(Figure 7D)** . These results highlight the importance of protein prenylation to HPV infection. Moreover, GGTI-298 inhibited LIMK1/cofilin phosphorylation, which is also evidence of prenylation affecting HPV-induced cytoskeletal reorganization **(Figure 7E)** .

Discussion

Despite preventions, such as HPV screening and vaccination, HPV infection burden remains heavy worldwide, owing to the paucity of treatments. This difficult situation might result from poor understanding of the HPV infection process. Therefore, we conceived this study to explore a broad-spectrum inhibitor for various pathogenic HPV types, providing, in parallel, traits of the HPV mode of infection.

25HC, a lipid oxysterol, has emerged as a powerful antiviral product of ISG. The antiviral properties of 25HC have been extensively studied in enveloped viruses. For instance, 25HC might 1) deprive cholesterol from cell membrane to hamper virus fusion, 2) block membrane web formation to prevent RNA replication, or 3) positively regulate adaptive immunity (4, 19-21). The inhibiting phenotype of 25HC has also been identified in several non-enveloped viruses, including HPV16, human rotavirus and human rhinovirus (HrHV)(22-24). However, the intrinsic mechanisms have not been thoroughly investigated. In this study, our HPV PsV inhibition assay suggested a broad-spectrum inhibitory phenotype of 25HC in cervical epithelial cells towards high-risk (HPV16, HPV18, HPV59), possibly carcinogenic (HPV73) and low-risk (HPV6) HPVs **(Figure 1)** .

Actin network is almost always the first-line cytoskeletal component encountered by viruses during the process of infection. On the one hand, dense cortical actin meshwork beneath the cell membrane acts as a physical barrier against virus invasion; on the other hand, viruses might hijack actin fibers to facilitate their entry into cytoplasm (25). Microfilaments are involved in viral attachment, internalization, transportation, budding and releasing. For example, coronavirus induces filopodia to facilitate internalization through macropinocytosis (26). Classical swine fever virus (CSFV) promotes microfilament reorganization by activating the EGFR-PI3K/MAPK-RhoA/Rac1/Cdc42 signaling axis and employs stress fibers to sustain CSFV trafficking in early and late endosomes (27). Cofilin-mediated F-actin dynamics is crucial for replication of intracellular herpes simplex virus 1 (HSV1)(20). Filopodia shuffle human respiratory syncytial virus (RSV) to nearby uninfected cells, driving virus spread (28). Ebolavirus, Marburg virus and HIV all depend on filopodia to release from host cells (29-32).

Virion surfing is a typical mechanism for viruses to make use of actin to break through the cell surface. During this process, long, finger-like filopodia protrude from the cell surface; virions interact with the cell membrane and bind to cellular receptors with high affinity. Consequently, virions are transported along filopodia towards the cell body in a membrane fusion or endocytic manner (12). Several findings support the idea that HPV uptake relies on this kind of translocation system. Smith reported in 2008 that cortical actin meshwork and stress fibers in human keratinocytes broke down immediately upon exposure to HPV31. A few minutes later, a strong induction of filopodia was observed, and HPV31 was internalized along this actin protrusion retrograde flow (13). Shortly afterwards, it was revealed that HPV16 surfing is sensitive to perturbations of actin dynamics (11). Using confocal imaging, we show that HPV16 PsV activated filopodia within 5 min, which is in accordance with previous studies**(Figure 4B)** . However, 25HC surprisingly inhibited formation of filopodia upon HPV16 PsV infection **(Figure 4C)** . We revealed a new target of 25HC antivirus effect, which triggers the cytoskeleton.

Highly dynamic polymerization and depolymerization remodel actin filaments into functional structures, such as filopodia, lamellipodia, stress fibers and microvilli. These structures are modified by exquisite regulation of ABPs and upstream signaling(33, 34). We found that a typical actin reorganization signaling pathway, LIMK/cofilin, might be involved in 25HC cytoskeletal regulation. We observed activated LIMK/cofilin signaling upon HPV16 PsV exposure, whereas 25HC suppressed LIMK and cofilin phosphorylation **(Figure 5A)** . Cofilin is expected to sever actin filament at a low cofilin/actin ratio, but stabilize actin filament at a high cofilin/actin ratio (35). In any case, ectopic activation of cofilin perturbs the process of virus entry (36).

Prenylation is a post-translational modification, endowing proteins with hydrophobic properties and allowing their attachment to cell membranes. A growing number of studies indicate that prenylation could be a target of virus inhibition. Disruption of large delta hepatitis antigen (L-DHAg) prenylation impedes hepatitis D virus (HDV) assembly (37). Oral prenylation inhibition with lonafarnib significantly reduced virus levels of chronic HDV infection in clinical trials (38). In other viruses, targets of prenylation could be located in host cell proteins. Inhibition of host protein geranylgeranylation disrupts hepatitis C virus (HCV) replication. This inhibitory effect might be related to Rab proteins (39). Blocking RhoA prenylation interrupts HIV envelope fusion with cell membranes (40). Loss of Rac1 prenylation represses expression of RSV fusion glycoprotein (F-protein) on the cell surface and strongly restricts infectious virus production (41). Taken together, prenylation inhibitors might be a novel class of antiviral agents.

Rho family and Ras family are typically prenylated, and they are broadly reported to be modulators of actin dynamics. Activation of Rho GTPases makes a significant contribution to viral entry, replication and spread. It has been shown that hepatitis E virus (HEV) exploits the Cdc42/p21-activated kinase1/cofilin pathway to facilitate virus infection (42). The US3 protein of pseudorabies virus (PDV) interferes with Rho GTPase signaling and causes reorganization of host cytoskeleton, which, as a consequence, enhances PDV cell-to-cell spread (43). Encephalitic alphavirus activates Rho GTPases within brain endothelium to break through the blood-brain barrier and enter the central nervous system (44). Rho inhibitors show potential for restoring infection of a wide array of viruses, including RSV and human parainfluenza virus (HPIV)(14,

41). Rap1 is member of the Ras subfamily involved in cytoskeletal dynamics (45). The mechanism of this actin coordination efficacy is correlated with the LIMK/cofilin pathway. It is observed that avian HEV upregulates and activates Rap1 during infection and consequently rearranges the cytoskeleton to promote virus internalization by permissive cells (46). Our data show that 25HC decreased active Rho GTPases and Rap1 levels in cervical epithelial cells, most likely through its restriction of isoprenoid synthesis**(Figure 5D, Figure 6)** . Our findings support that small GTPase prenylation could be a promising target for HPV infection.

In this work, we have described the broad-spectrum anti-HPV effect of 25HC and its likely mediation through reprogramming of isoprenoid metabolism and cytoskeletal rearrangement. 25HC inhibits biosynthesis of protein prenylation substrates, FPP and GGPP, thereby affecting membrane/cytoplasm location of small GTPases and disturbing their interaction by downstream signaling. As a result, the LIMK/cofilin pathway is suppressed, and F-actin rearrangement is impeded. Consequently, HPV infection is restrained owing to failed virion surfing**(Figure 8)** .

The present study provides, for the first time, evidence for the broad-spectrum anti-HPV efficacy of 25HC. We first describe that 25HC inhibits HPV infection via a lipid metabolism-related mechanism, involving prenylation of small GTPases. We also discover the regulatory capacity of 25HC vis-à-vis the cytoskeleton, yielding new targets for 25HC antiviral exploration. Overall, 25HC could be a potential therapeutic agent to control HPV infection in future clinical applications. However, because the PsV system only mimics the entry process of HPV, our study did not probe the effects of 25HC on other processes of the viral life cycle. In-depth research using diverse types of methods, including murine papillomavirus model and cervical raft culture, can help depict the complete picture of 25HC's anti-HPV capability.

Acknowledgement

We thank Q. Wang at Shanghai Medical College, Fudan University for technical support.

Conflict of Interest Disclosure

The authors declare no competing interests.

Funding Statement

This work was supported in part by funding from Natural Science Foundation of Shanghai (22ZR1408800) and Shanghai Municipal Science and Technology Major Project (ZD2021CY001).

Data availability Statement

The data that support the findings of this study are available on request from the corresponding author.

References

1. Schiffman M, Doorbar J, Wentzensen N, de Sanjose S, Fakhry C, Monk BJ, et al. Carcinogenic human papillomavirus infection. Nat Rev Dis Primers. 2016;2.

2. Lei JY, Ploner A, Elfstrom KM, Wang JR, Roth A, Fang F, et al. HPV Vaccination and the Risk of Invasive Cervical Cancer. New Engl J Med. 2020;383(14):1340-8.

3. Cohen PA, Jhingran A, Oaknin A, Denny L. Cervical cancer. Lancet. 2019;393(10167):169-82.

4. Blanc M, Hsieh WY, Robertson KA, Kropp KA, Forster T, Shui G, et al. The transcription factor STAT-1 couples macrophage synthesis of 25-hydroxycholesterol to the interferon antiviral response. Immunity. 2013;38(1):106-18.

5. Liu SY, Aliyari R, Chikere K, Li GM, Marsden MD, Smith JK, et al. Interferon-Inducible Cholesterol-25-Hydroxylase Broadly Inhibits Viral Entry by Production of 25-Hydroxycholesterol. Immunity. 2013;38(1):92-105.

6. Zeng RC, Case JB, Yutuc E, Ma XC, Sheng S, Castro MFG, et al. Cholesterol 25-hydroxylase suppresses SARS-CoV-2 replication by blocking membrane fusion. P Natl Acad Sci USA. 2020;117(50):32105-13.

7. Hua C, Zhu Y, Wu CQ, Si LL, Wang Q, Sui L, et al. The Underlying Mechanism of 3-Hydroxyphthalic Anhydride-Modified Bovine Beta-Lactoglobulin to Block Human Papillomavirus Entry Into the Host Cell. Front Microbiol. 2019;10.

8. Lu L, Pan C, Li Y, Lu H, He W, Jiang S. A bivalent recombinant protein inactivates HIV-1 by targeting the gp41 prehairpin fusion intermediate induced by CD4 D1D2 domains. Retrovirology. 2012;9:104.

9. Roberts JN, Buck CB, Thompson CD, Kines R, Bernardo M, Choyke PL, et al. Genital transmission of HPV in a mouse model is potentiated by nonoxynol-9 and inhibited by carrageenan. Nat Med. 2007;13(7):857-61.

10. Roden RBS, Stern PL. Opportunities and challenges for human papillomavirus vaccination in cancer. Nat Rev Cancer. 2018;18(4):240-54.

11. Schelhaas M, Ewers H, Rajamaki ML, Day PM, Schiller JT, Helenius A. Human papillomavirus type 16 entry: Retrograde cell surface transport along actin-rich protrusions. Plos Pathog. 2008;4(9).

12. Taylor MP, Koyuncu OO, Enquist LW. Subversion of the actin cytoskeleton during viral infection. Nat Rev Microbiol. 2011;9(6):427-39.

13. Smith JL, Lidke DS, Ozbun MA. Virus activated filopodia promote human papillomavirus type 31 uptake from the extracellular matrix. Virology. 2008;381(1):16-21.

14. Wang JC, Lee JYJ, Christian S, Dang-Lawson M, Pritchard C, Freeman SA, et al. The Rap1-cofilin-1 pathway coordinates actin reorganization and MTOC polarization at the B cell immune synapse. J Cell Sci. 2017;130(6):1094-109.

15. Crosas-Molist E, Samain R, Kohlhammer L, Orgaz JL, George SL, Maiques O, et al. Rho GTPase signaling in cancer progression and dissemination. Physiol Rev. 2022;102(1):455-510.

16. Zhao J, Chen J, Li M, Chen M, Sun C. Multifaceted Functions of CH25H and 25HC to Modulate the Lipid Metabolism, Immune Responses, and Broadly Antiviral Activities. Viruses. 2020;12(7).

17. Jiang H, Zhang X, Chen X, Aramsangtienchai P, Tong Z, Lin H. Protein Lipidation: Occurrence, Mechanisms, Biological Functions, and Enabling Technologies. Chem Rev. 2018;118(3):919-88.

18. Xu N, Guan S, Chen Z, Yu Y, Xie J, Pan FY, et al. The alteration of protein prenylation induces cardiomyocyte hypertrophy through Rheb-mTORC1 signalling and leads to chronic heart failure. J Pathol. 2015;235(5):672-85.

19. Li CF, Deng YQ, Wang S, Ma F, Aliyari R, Huang XY, et al. 25-Hydroxycholesterol Protects Host against Zika Virus Infection and Its Associated Microcephaly in a Mouse Model. Immunity. 2017;46(3):446-56.

20. Anggakusuma, Romero-Brey I, Berger C, Colpitts CC, Boldanova T, Engelmann M, et al. Interferon-inducible cholesterol-25-hydroxylase restricts hepatitis C virus replication through blockage of membranous web formation. Hepatology. 2015;62(3):702-14.

21. Wu TJ, Ma F, Ma XC, Jia WZ, Pan EX, Cheng GH, et al. Regulating Innate and Adaptive Immunity for Controlling SIV Infection by 25-Hydroxycholesterol. Front Immunol. 2018;9.

22. Civra A, Cagno V, Donalisio M, Biasi F, Leonarduzzi G, Poli G, et al. Inhibition of pathogenic non-enveloped viruses by 25-hydroxycholesterol and 27-hydroxycholesterol. Sci Rep-Uk. 2014;4.

23. Arita M, Kojima H, Nagano T, Okabe T, Wakita T, Shimizu H. Oxysterol-Binding Protein Family I Is the Target of Minor Enviroxime-Like Compounds. J Virol. 2013;87(8):4252-60.

24. Roulin PS, Lotzerich M, Torta F, Tanner LB, van Kuppeveld FJM, Wenk MR, et al. Rhinovirus Uses a Phosphatidylinositol 4-Phosphate/Cholesterol Counter-Current for the Formation of Replication Compartments at the ER-Golgi Interface. Cell Host Microbe. 2014;16(5):677-90.

25. Walsh D, Naghavi MH. Exploitation of Cytoskeletal Networks during Early Viral Infection. Trends Microbiol. 2019;27(1):39-50.

26. Freeman MC, Peek CT, Becker MM, Smith EC, Denison MR. Coronaviruses Induce Entry-Independent, Continuous Macropinocytosis. Mbio. 2014;5(4).

27. Cheng Y, Lou JX, Liu CC, Liu YY, Chen XN, Liang XD, et al. Microfilaments and Microtubules Alternately Coordinate the Multistep Endosomal Trafficking of Classical Swine Fever Virus. J Virol. 2021;95(10).

28. Mehedi M, McCarty T, Martin SE, Le Nouen C, Buehler E, Chen YC, et al. Actin-Related Protein 2 (ARP2) and Virus-Induced Filopodia Facilitate Human Respiratory Syncytial Virus Spread. Plos Pathog. 2016;12(12):e1006062.

29. Schudt G, Dolnik O, Kolesnikova L, Biedenkopf N, Herwig A, Becker S. Transport of Ebolavirus Nucleocapsids Is Dependent on Actin Polymerization: Live-Cell Imaging Analysis of Ebolavirus-Infected Cells. J Infect Dis. 2015;212:S160-S6.

30. Dolnik O, Kolesnikova L, Welsch S, Strecker T, Schudt G, Becker S. Interaction with Tsg101 Is Necessary for the Efficient Transport and Release of Nucleocapsids in Marburg Virus-Infected Cells. Plos Pathog. 2014;10(10).

31. Aggarwal A, Stella AO, Henry CC, Narayan K, Turville SG. Embedding of HIV Egress within Cortical F-Actin. Pathogens. 2022;11(1).

32. Do T, Murphy G, Earl LA, Del Prete GQ, Grandinetti G, Li GH, et al. Three-Dimensional Imaging of HIV-1 Virological Synapses Reveals Membrane Architectures Involved in Virus Transmission. J Virol. 2014;88(18):10327-39.

33. De Conto F, Fazzi A, Razin SV, Arcangeletti MC, Medici MC, Belletti S, et al. Mammalian Diaphanous-related formin-1 restricts early phases of influenza A/NWS/33 virus (H1N1) infection in LLC-MK2 cells by affecting cytoskeleton dynamics. Mol Cell Biochem. 2018;437(1-2):185-201.

34. Kloc M, Uosef A, Wosik J, Kubiak JZ, Ghobrial RM. Virus interactions with the actin cytoskeleton-what we know and do not know about SARS-CoV-2. Arch Virol. 2022;167(3):737-49.

35. Xiang YF, Zheng K, Ju HG, Wang SX, Pei Y, Ding WC, et al. Cofilin 1-Mediated Biphasic F-Actin Dynamics of Neuronal Cells Affect Herpes Simplex Virus 1 Infection and Replication. J Virol. 2012;86(16):8440-51.

36. Lv XL, Li Z, Guan JY, Hu SY, Zhang J, Lan YG, et al. Porcine Hemagglutinating Encephalomyelitis Virus Activation of the Integrin alpha 5 beta 1-FAK-Cofilin Pathway Causes Cytoskeletal Rearrangement To Promote Its Invasion of N2a Cells. J Virol. 2019;93(5).

37. Liang YJ, Sun CP, Hsu YC, Chen YW, Wang IA, Su CW, et al. Statin inhibits large hepatitis delta antigen-Smad3 -twist-mediated epithelial-to-mesenchymal transition and hepatitis D virus secretion. J Biomed Sci. 2020;27(1):65.

38. Koh C, Canini L, Dahari H, Zhao XC, Uprichard SL, Haynes-Williams V, et al. Oral prenylation inhibition with lonafarnib in chronic hepatitis D infection: a proof-of-concept randomised, double-blind, placebo-controlled phase 2A trial. Lancet Infect Dis. 2015;15(10):1167-74.

39. Ye J, Wang CF, Sumpter R, Brown MS, Goldstein JL, Gale M. Disruption of hepatitis C virus RNA replication through inhibition of host protein geranylgeranylation. P Natl Acad Sci USA. 2003;100(26):15865-70.

40. del Real G, Jimenez-Baranda S, Mira E, Lacalle RA, Lucas P, Gomez-Mouton C, et al. Statins inhibit HIV-1 infection by down-regulating Rho activity. J Exp Med. 2004;200(4):541-7.

41. Malhi M, Norris MJ, Duan WM, Moraes TJ, Maynes JT. Statin-mediated disruption of Rho GTPase prenylation and activity inhibits respiratory syncytial virus infection. Commun Biol. 2021;4(1).

42. Fan MN, Luo YH, Zhang BB, Wang JX, Chen TX, Liu BY, et al. Cell Division Control Protein 42 Interacts With Hepatitis E Virus Capsid Protein and Participates in Hepatitis E Virus Infection. Front Microbiol. 2021;12.

43. Lamote JAS, Glorieux S, Nauwynck HJ, Favoreel HW. The US3 Protein of Pseudorabies Virus Drives Viral Passage across the Basement Membrane in Porcine Respiratory Mucosa Explants. J Virol. 2016;90(23):10945-50.

44. Salimi H, Cain MD, Jiang XP, Roth RA, Beatty WL, Sun CQ, et al. Encephalitic Alphaviruses Exploit Caveola-Mediated Transcytosis at the Blood-Brain Barrier for Central Nervous System Entry. Mbio. 2020;11(1).

45. Zhang X, Cao S, Barila G, Edreira MM, Hong K, Wankhede M, et al. Cyclase-associated protein 1 (CAP1) is a prenyl-binding partner of Rap1 GTPase. J Biol Chem. 2018;293(20):7659-73.

46. Zhang BB, Fan MN, Fan J, Luo YH, Wang J, Wang YJ, et al. Avian Hepatitis E Virus ORF2 Protein Interacts with Rap1b to Induce Cytoskeleton Rearrangement That Facilitates Virus Internalization. Microbiol Spectr. 2022;10(1).

Figure legends

Figure 1. Broad-spectrum antiviral activity of 25HC against HPV PsV. (A) Infected HeLa (a) and C-33A cells (b) were treated for 16 h with increasing concentrations of 25HC. The percentage of infection was calculated by comparing treated and untreated cells. The results were shown in means, and standard curves were drawn using nonlinear regression. (B) HeLa cells were infected with HPV16 PsV in the absence (a) or presence (b) of 25HC. Cells were harvested at 2 hours post-infection and then stained with anti-HPV16 L1 antibody and DAPI. HPV16 PsV virions were dramatically decreased in 25HC-treated cells. (Scale bar = 100 μm)

Figure 2. Protection against *in vivo* genital challenge with HPV16 PsV by 25HC. (A) Groups of mice were intravaginally challenged with HPV16 PsV. Mice were treated with 25HC intravaginally. Bioluminescence was visualized with a Xenogen camera. No mice were infected in the 25HC-treated group. (B) Bioluminescence of genital area was measured in p/s. The luminescence value had significantly decreased in the 25HC-treated group. (NS, non-significance; *, $p < 0.05$; **, $p < 0.01$; ***, $p < 0.001$).

Figure 3. 25HC targets cervical epithelial cells, but not virions, at an early stage of HPV infection. (A) Schemes of time-of-addition assay (a) and pretreatment assay (b). (B) HPV16 PsV was incubated with 25HC and then separated by ultrafiltration before being added to HeLa cells. 25HC could not inactivate HPV16 PsV. (C) In the time-of-addition assay, HeLa cells were incubated with HPV PsVs, and 25HC was added at different times. The inhibitory activity sharply decreased at 2 h post-infection. (D) HeLa cells were treated with 25HC of different concentrations for 12 h and washed before HPV PsV inoculation. HPV infection was inhibited by 25HC pretreatment in a dose-dependent manner. (E) HeLa cells were treated with 25HC for different time periods and washed, followed by inoculation with HPV PsV. HPV infection was inhibited by 25HC pretreatment in a time-dependent manner.

Figure 4. 25HC perturbs cytoskeletal reorganization at an early stage of HPV infection. (A) F-actin was evaluated by phalloidin coupled with rhodamine. In uninfected HeLa cells, F-actin was distributed diffusely. (B) Exposure to HPV16 PsV caused abundant filopodia to form within 5 min post-infection. 2 h post-infection, filopodia broke down. (C) In the presence of 25HC, HeLa cells could not induce strong

filopodia activation upon HPV16 PsV exposure. (63× objective, scale bar = 25 μm; zoom, scale bar = 7.5 μm; arrow: typical filopodium structure).

Figure 5. 25HC suppresses small molecular weight GTPase activity, resulting in inhibition of LIMK/cofilin phosphorylation activity during HPV infection. (A) Proteins of HeLa cells were collected at different time points post-HPV16 PsV infection for Western blot evaluation. Phosphorylated LIMK1 was increased by HPV inoculation. Cofilin phosphorylation also increased within 5 min post-infection, but decreased after 2 h. However, in 25HC-treated cells, at each time point, phosphorylation levels of LIMK1 and cofilin were lower than those observed in the control group. β-actin was used as loading control. (B)(C) Grayscale values of the Western blots were evaluated. Relative intensity of p-cofilin and p-LIMK1 was normalized to β-actin and standardized relative to mock of the control group. The differences between control group and 25HC group at each time point were calculated. Data are shown as the mean ± SD. (NS, non-significance; *, $p < 0.05$; **, $p < 0.01$; ***, $p < 0.001$). (D) Equal amounts of HeLa cell lysates in the absence or presence of 25HC were used to capture the GTP-bound form of Rho GTPases (Rac1, Cdc42, RhoA) by affinity precipitation with GST-PBD beads and capture GTP-bound Rap1 by active Rap1 GTP monoclonal antibody. The active GTP-bound forms of Rac1, Cdc42, RhoA and Rap1 were reduced by 25HC treatment.

Figure 6. 25HC inhibits biosynthesis of small GTPase prenylation substrates. (A) 67 DEGs were identified from RNA-seq of 25HC-treated or untreated HeLa cells. (B) 2 gene sets were enriched in DEGs using KEGG annotation analysis. (C) The top 20 gene sets enriched by GO analysis were mainly lipid metabolism-related. (D) Isoprenoid biosynthetic process was enriched according to GSEA analysis. (E) Gene expressions from RNA-seq data were analyzed. Genes in the "isoprenoid biosynthetic process" set were mainly downregulated in the 25HC group. The differences between the control group and 25HC groups were calculated. Data are shown as the mean ± SD. (NS, non-significance; *, $p < 0.05$; **, $p < 0.01$; ***, $p < 0.001$) (F) Genes of MVA key enzymes were downregulated by 25HC, according to RNA-seq data. (G) qPCR was applied to estimate the expression of FDPS and GGPPS. The differences between the control group and 25HC group were calculated. Data are shown as the mean ± SD. (NS, non-significance; *, $p < 0.05$; **, $p < 0.01$; ***, $p < 0.001$).

Figure 7. 25HC suppresses HPV infection by restricting small GTPase prenylation. (A) Pan-prenylation level was suppressed by 25HC. (B) Membrane proteins were collected for Western blot. Membrane-bound, prenylated Rac1, Cdc42, RhoA and Rap1 expressions were reduced by 25HC. Na^+/K^+ ATPase (ATP1a1) was used as membrane loading control. (C) The prenylation inhibitors (a) GGTI-298 and (b) FTI-277 revealed anti-HPV16 PsV effect in inhibitory assays. (D) Farnesylation substrate FPP rescued anti-HPV capability of 25HC. (E) Prenylation inhibitor GGTI-298 inhibited LIMK1/cofilin phosphorylation.

Figure 8. Mechanism of 25HC anti-HPV effect in cervical epithelial cells. FPP and GGPP are substrates for protein prenylation. Prenylation of small GTPases enables their binding to cellular membranes and their ability to function as a signal switch. The downstream LIMK/cofilin pathway is thereby phosphorylated to dynamically regulate the balance between actin assembly/disassembly. This allows filopodia to protrude from the cell membrane, and HPV virions make use of this structure to invade cervical epithelial cells. However, 25HC inhibits FPP and GGPP biosynthesis, consequently impeding HPV infection.

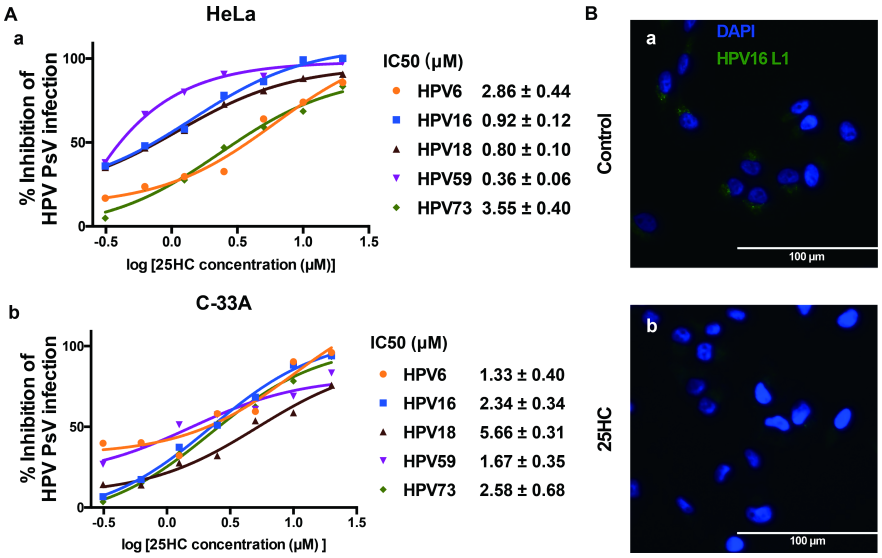

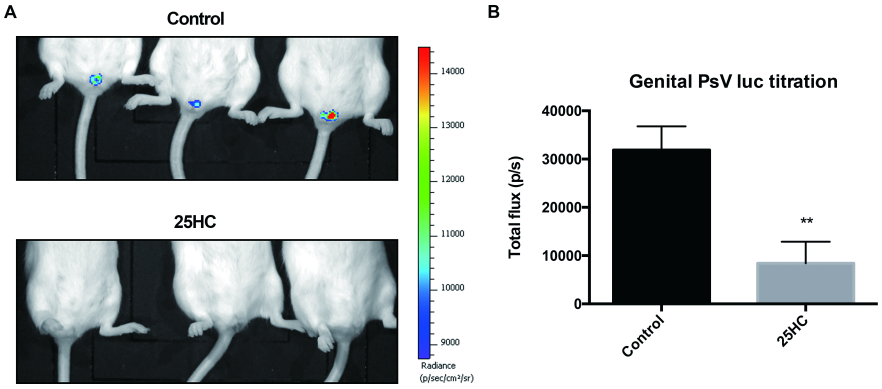

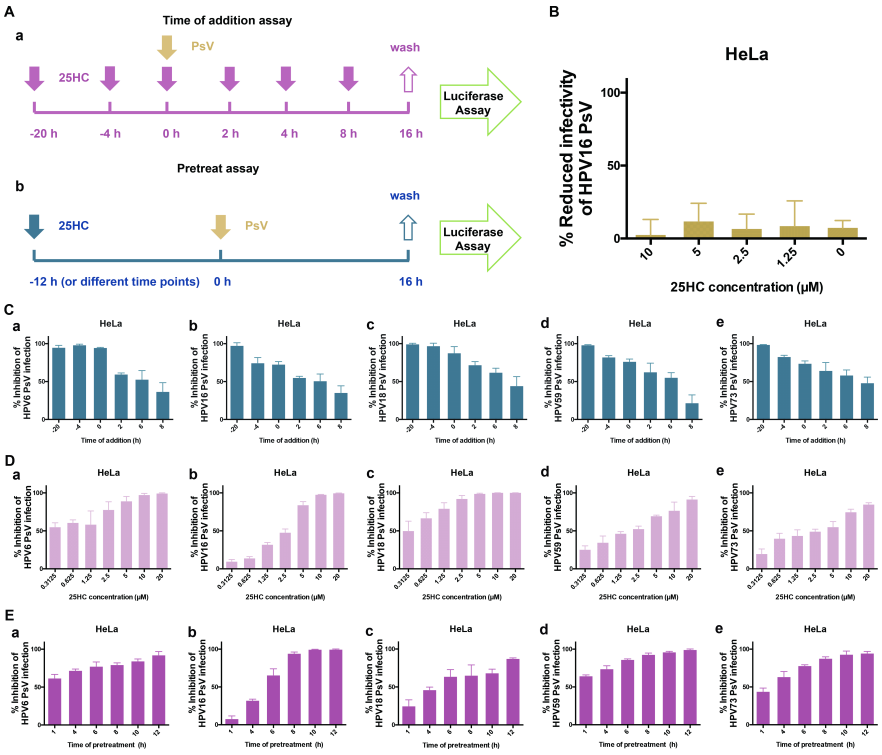

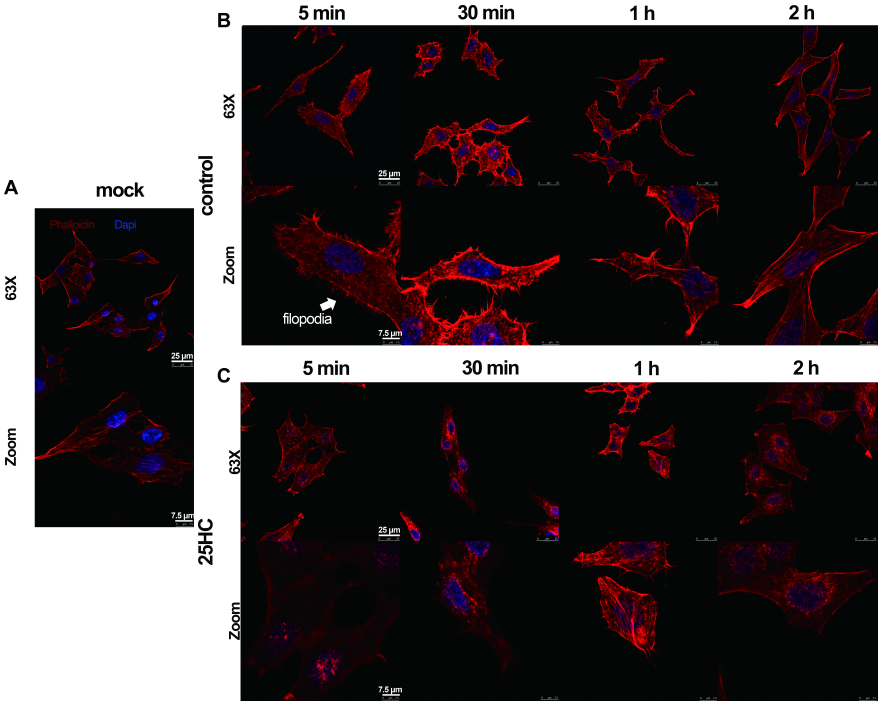

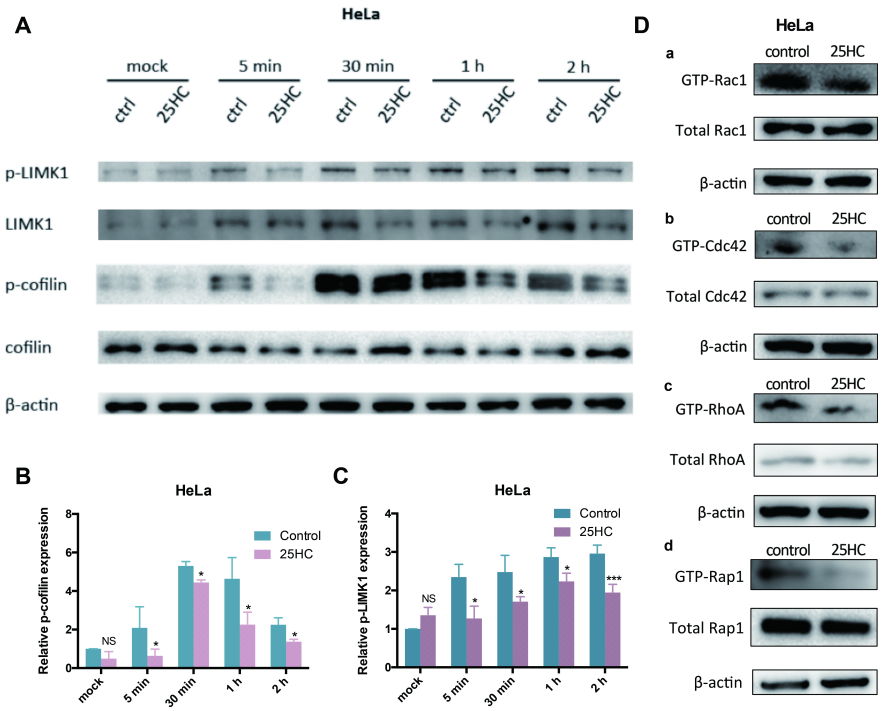

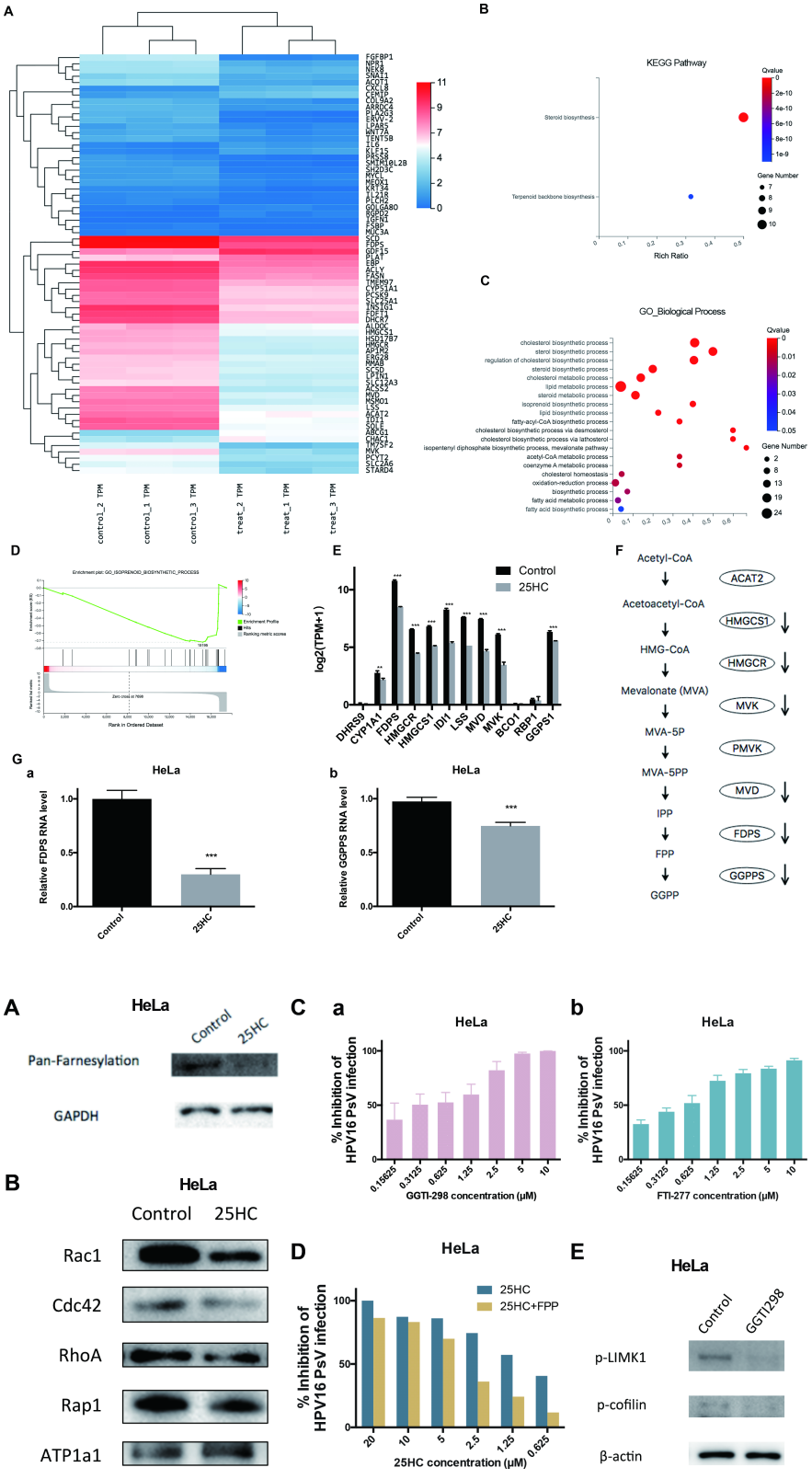

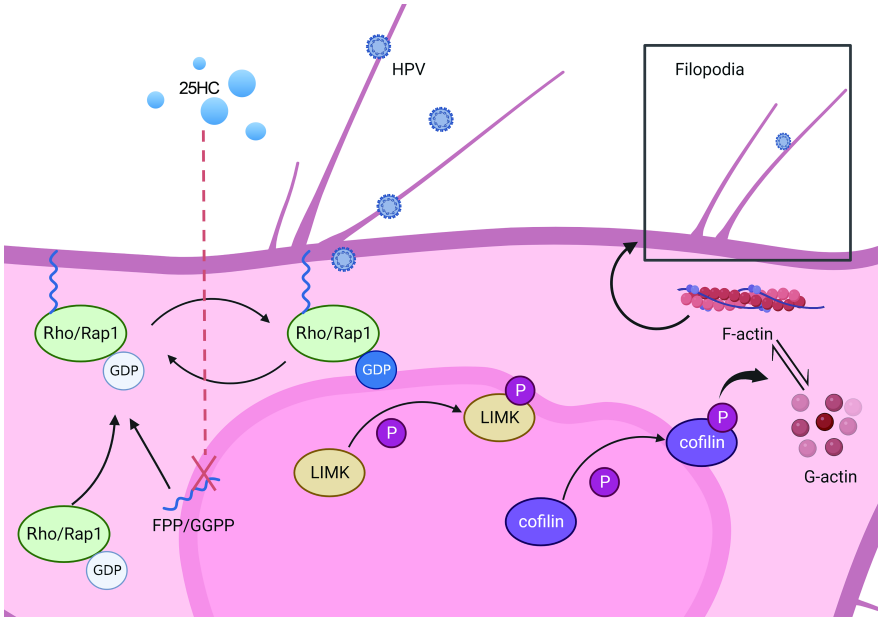

Hosted file

Table 1.docx available at https://authorea.com/users/580240/articles/621383-25-hydroxycholesterol-inhibits-human-papillomavirus-infection-in-cervical-epithelial-cells-by-perturbing-cytoskeletal-remodeling